

# A Neural-enhanced Factor Graph-based Algorithm for Robust Positioning in Obstructed LOS Situations

Alexander Venus<sup>1,2</sup>, Erik Leitinger<sup>1,2</sup>, Stefan Tertinek<sup>3</sup>, and Klaus Witrisal<sup>1,2</sup>

<sup>1</sup>Graz University of Technology, Austria, <sup>3</sup>NXP Semiconductors, Austria,

<sup>2</sup>Christian Doppler Laboratory for Location-aware Electronic Systems

**Abstract**—This paper presents a neural-enhanced probabilistic model and corresponding factor graph-based sum-product algorithm for robust localization and tracking in multipath-prone environments. The introduced hybrid probabilistic model consists of physics-based and data-driven measurement models capturing the information contained in both, the line-of-sight (LOS) component as well as in multipath components (NLOS components). The physics-based and data-driven models are embedded in a joint Bayesian framework allowing to derive from first principles a factor graph-based algorithm that fuses the information of these models. The proposed algorithm uses radio signal measurements from multiple base stations to robustly estimate the mobile agent’s position together with all model parameters. It provides high localization accuracy by exploiting the position-related information of the LOS component via the physics-based model and robustness by exploiting the geometric imprint of multipath components independent of the propagation channel via the data-driven model. In a challenging numerical experiment involving obstructed LOS situations to all anchors, we show that the proposed sequential algorithm significantly outperforms state-of-the-art methods and attains the posterior Cramér-Rao lower bound even with training data limited to local regions.

**Index Terms**—Obstructed Line-Of-Sight, Non LOS, NLOS, Multipath, Sum product algorithm, Probabilistic Data Association, Belief Propagation

## I. INTRODUCTION

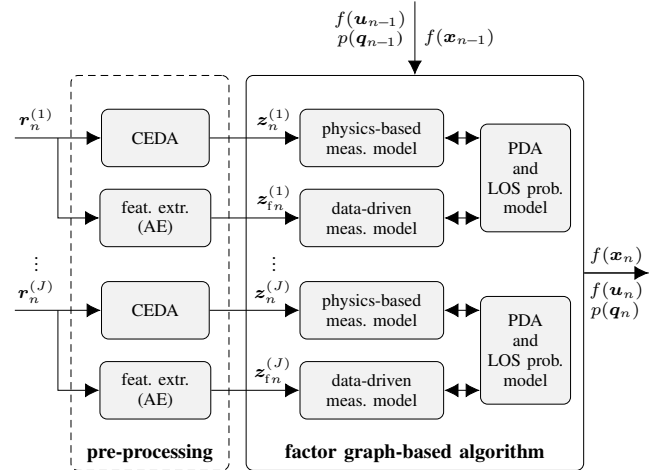
Localization of mobile agents using radio signals is still a challenging task in environments such as indoor or urban territories [1]–[3]. These environments are characterized by strong multipath propagation and frequent obstructed line-of-sight (OLOS) situations, which can prevent the correct extraction of information contained in the line-of-sight (LOS) component<sup>1</sup>. There exist many safety- and security-critical applications, such as autonomous driving [4], medical services [5], or keyless entry systems [6], where robustness of the position estimate (i.e., no lost tracks) is of critical importance.

### A. State-of-the-Art Methods

New localization and tracking approaches within the context of 6G localization [7] take advantage of large measurement

The financial support by the Christian Doppler Research Association, the Austrian Federal Ministry for Digital and Economic Affairs and the National Foundation for Research, Technology and Development is gratefully acknowledged.

<sup>1</sup>Throughout this paper we use the terms “multipath component (MPC)” and “NLOS components” interchangeably to refer to all received signal components except the LOS component. Also, we use the term “obstructed LOS” (OLOS), to refer to situations, where the LOS component is blocked or cannot be detected. We distinguish between partial and full OLOS situations, where the LOS component of some or all anchors is unavailable.



CEDA	channel estimation and detection algorithm
feat. extr. (AE)	autoencoder-based feature extraction
physics-based meas. model	physics-based measurement model that facilitates the LOS component
data-driven meas. model	data-driven measurement model that facilitates NLOS propagation using Gaussian process regression (GPR)
factor graph-based algorithm	joint Bayesian inference using the sum-product algorithm (SPA)
PDA	probabilistic data association involving both, the physics-based and the data-driven measurement model
LOS prob. model	dynamic model for the LOS existence probability

Fig. 1. Flowchart illustrating the main components of the proposed method. For each base station  $j \in \{1, \dots, J\}$  we observe a baseband radio signal vector  $\mathbf{r}_n^{(j)}$  which is independently pre-processed into signal component measurements  $\mathbf{z}_n^{(j)}$  (LOS component and MPCs) and feature measurements  $\mathbf{z}_{fn}^{(j)}$ . The factor graph-based algorithm uses these measurements and the distributions of agent state, amplitude state, and LOS probability state at the previous time step, given as  $f(\mathbf{x}_{n-1})$ ,  $f(\mathbf{u}_{n-1})$ ,  $p(\mathbf{q}_{n-1})$ , to infer the posterior distributions  $f(\mathbf{x}_n)$ ,  $f(\mathbf{u}_n)$ ,  $p(\mathbf{q}_n)$  at the current time step. For simplicity, we omit conditional dependencies of the distributions.

apertures as ultra wide band (UWB) systems [8], [9] or mmWave systems [10], which allow the received radio signal to be resolved into a superposition of a finite number of specular multipath components (MPCs) [8], [11]–[13]. Such novel approaches try to mitigate the effect of multipath propagation [14] and OLOS situations [13], [15] or even take advantage of MPCs by exploiting inherent position information, turning multipath from impairment to an asset [1], [16], [17]. Prominent examples of such approaches are multipath-based methods that take advantage of multipath by estimating MPCs and associating them to virtual anchors (VAs) representing the location of the mirror image of a base station (anchor) on a reflecting surface. The locations of VAs are assumed to be known a priori [18] or estimated jointly with the position

of the agent using multipath-based SLAM (MP-SLAM) [16], [19], [20]. MP-SLAM provides high-accuracy position estimates even in OLOS situations. However, it requires specular, resolved MPCs caused by environments consistent with the VA model, i.e, flat surfaces of sufficient extend [21]–[23]. Other methods exploit cooperation among individual agents [3], [24], [25], or perform robust signal processing against multipath propagation and clutter measurements in general. The latter comprise heuristics [8], [26], machine learning-based approaches [15], [27] as well as Bayesian methods [23], [28]–[30], and hybrids thereof [3], [31]–[33]. In particular, the methods introduced in [34] and [23], [29], [30] perform MP-SLAM or robust positioning considering delay dispersion and non-resolvable dense MPC [22]. In recent years, machine learning-based approaches have grown increasingly popular. Typically, they extract specific features from the radio channel, applying model-agnostic supervised regression methods on these features [15], [27]. While these approaches potentially provide high accuracy estimates at low computational demand (after training), they suffer from their dependence on a large representative measurement database and can fail in scenarios that are not sufficiently represented by the training data. This is why recent algorithms facilitate deep learning and autoencoder-based, unsupervised methods [35]–[40] or try to incorporate physics-based information in a systematic manner [41]–[44] to reduce the dependence on training data .

Multipath-based localization [16], [19], [23], [45], multiobject-tracking [46]–[48], and parametric channel tracking [49] are applications that pose common challenges such as for example uncertainties beyond Gaussian noise, like missed detections and clutter, an uncertain origin of measurements, and unknown and time-varying numbers of objects to be localized and tracked. These challenges are well addressed by Bayesian inference leveraging graphical models to perform joint detection and estimation. In particular, the probabilistic data association (PDA) algorithm [46], [50] represents a low-complexity Bayesian method for robust localization and tracking with extension to multiple-sensors PDA [51] and amplitude information [52].

### B. Problem Statement and Contributions

The problem studied in this paper can be summarized as follows.

*Estimate the time-varying location of a mobile agent using LOS propagation and multipath propagation of radio signals with emphasis on overcoming OLOS situations.*

We propose a neural-enhanced sum-product algorithm (SPA) for robust radio signal-based localization and tracking in multipath-prone environments. The proposed algorithm performs joint probabilistic data association and sequential estimation of a mobile agent state together with all relevant model-parameters (amplitude state, LOS probability, data association variable) using message passing by means of the SPA on a factor graph [53]. The main components of the proposed algorithm are illustrated in the flowchart provided in Fig. 1. We introduce a hybrid physics-based and data-driven model, which allows the proposed sequential algorithm to leverage the

information contained in both, the LOS component and MPCs (NLOS components) of multiple base stations to robustly estimate the mobile agent’s position. Similar to other “two-step approaches” [16], [19], [47], [48], the proposed algorithm uses signal component measurements consisting of delays and corresponding amplitudes estimated out of the received baseband signal by a snapshot-based parametric channel estimation and detection algorithm (CEDA). Additionally, our hybrid method uses feature measurements extracted out of the received baseband signal by an autoencoder deep neural network (AE-DNN) [43], [54]. Using the measurements provided by the CEDA, our physics-based model allows the algorithm to facilitate the position-related information contained in the LOS component with high accuracy and without the need of training data. The data-driven model, which is based on Gaussian process regression (GPR) [55], uses the feature measurements extracted by the AE-DNN to leverage the complex position-related information inherently contained in multipath components regardless of the source of multipath (e.g. flat walls and point scatters, but also curved and rough walls as well as irregular objects such as shelves or pillars). The introduced physics-based and data-driven models interact through a joint probabilistic data association model [19], [47] and a dynamic LOS existence probability model [23], [56]. This allows the algorithm to robustly fuse the information contained in both, the LOS component and MPCs and, thus, to operate accurately and reliably within challenging environments, characterized by strong multipath propagation and OLOS situations.

The key contributions of this paper are as follows:

- We introduce a novel Bayesian model for MPC-aided sequential inference of the agent position consisting of a hybrid physics-based and data-driven measurement model.
- We present an SPA based on the factor graph representation of the estimation problem, which efficiently infers all parameters of the introduced joint probabilistic model.
- We demonstrate that our algorithm robustly and accurately fuses the information contained in the presented hybrid model. It outperforms state-of-the-art methods for non-LOS (NLOS) mitigation [15], [23], [43] and constantly attains the posterior Cramér-Rao lower bound (P-CRLB) [57].

## II. OVERVIEW

The problem considered is the sequential estimation of the agent state  $\mathbf{x}_n$ , while the agent is moving along an unknown trajectory. The current state of the agent is described by the state vector  $\mathbf{x}_n = [\mathbf{p}_n^T \mathbf{v}_n^T]^T$ , which is composed of the mobile agent’s position  $\mathbf{p}_n = [p_{xn} \ p_{yn}]^T$  and velocity  $\mathbf{v}_n = [v_{xn} \ v_{yn}]^T$ . At each discrete time  $n$ , the mobile agent transmits a signal and each anchor (base station)  $j \in \{1, \dots, J\}$  at anchor position  $\mathbf{p}_A^{(j)} = [p_{Ax}^{(j)} \ p_{Ay}^{(j)}]^T$  acts as a receiver. For each anchor, we obtain the complex baseband signal vector  $\mathbf{r}_n^{(j)} \in \mathbb{C}^{N_s}$  with  $N_s$  being the number of signal samples. Fig. 1 shows the main components of the proposed algorithm. In a pre-processing stage, we apply to  $\mathbf{r}_n^{(j)}$  both, a CEDA and an AE-DNN to obtain signal component measurements  $\mathbf{z}_n$  and feature measurements  $\mathbf{z}_{fn}$ , respectively. The agent state can be

sequentially estimated in a Bayesian sense using all available measurements  $\mathbf{z}_{1:n}, \mathbf{z}_{f1:n}$  of all anchors up to time  $n$  by using the minimum mean-square error (MMSE) estimator [58]

$$\hat{\mathbf{x}}_n^{\text{MMSE}} \triangleq \int \mathbf{x}_n f(\mathbf{x}_n | \mathbf{z}_{1:n}, \mathbf{z}_{f1:n}) d\mathbf{x}_n. \quad (1)$$

with  $\hat{\mathbf{x}}_n^{\text{MMSE}} = [\hat{\mathbf{p}}_n^{\text{MMSE T}} \hat{\mathbf{v}}_n^{\text{MMSE T}}]^T$  being the MMSE estimate.

The proposed factor graph-based algorithm infers the marginal posterior distribution  $f(\mathbf{x}_n | \mathbf{z}_{1:n}, \mathbf{z}_{f1:n})$  by executing the SPA on the factor graph that represents the hybrid probabilistic model introduced in this work. The structure of the following two sections, which present the introduced system model, aligns with the main components illustrated in Fig. 1.

### III. PRE-PROCESSING

#### A. Channel Estimation and Detection

We independently apply, at each time  $n$  and for each anchor  $j$ , a parametric CEDA [11], [23], [59], [60] to the complex baseband signal vector  $\mathbf{r}_n^{(j)}$ . The CEDA decomposes  $\mathbf{r}_n^{(j)}$  into individual components, yielding a number of  $M_n^{(j)}$  measurements denoted by  $\mathbf{z}_{m,n}^{(j)}$  with  $m \in \mathcal{M}_n^{(j)} \triangleq \{1, \dots, M_n^{(j)}\}$  that are collected by the vector  $\mathbf{z}_n^{(j)} = [\mathbf{z}_{1,n}^{(j)T} \dots \mathbf{z}_{M_n^{(j)},n}^{(j)T}]^T$ . Each  $\mathbf{z}_{m,n}^{(j)} = [z_{d_{m,n}^{(j)}}^{(j)} z_{u_{m,n}^{(j)}}^{(j)}]^T$  represents a signal component parameter estimate, containing a distance measurement  $z_{d_{m,n}^{(j)}}^{(j)} \in [0, d_{\max}]$  and a normalized amplitude measurement  $z_{u_{m,n}^{(j)}}^{(j)} \in [\gamma, \infty)$ , where  $d_{\max}$  is the maximum possible distance and  $\gamma$  is the detection threshold of the CEDA, which is a constant to be chosen<sup>2</sup>. Here, “normalized amplitude” refers to the square root of the signal-to-noise-ratio (SNR) of the signal component. See [49] for details on the signal model underlying a CEDA. The stacked vector  $\mathbf{z}_n = [\mathbf{z}_n^{(1)T} \dots \mathbf{z}_n^{(J)T}]^T$  is used by the proposed algorithm as a noisy measurement. We also define the vector  $\mathbf{M}_n = [M_n^{(1)} \dots M_n^{(J)}]^T$ .

#### B. AE-based Feature Extraction

At each time  $n$  and for each anchor  $j$  we independently apply a pre-trained autoencoder deep neural network (AE-DNN) [54], [61] where the complex baseband signal vector  $\mathbf{r}_n^{(j)}$  acts as the decoded input<sup>3</sup>. We use the mean squared error (MSE) between the training inputs and the predictions of the decoder network of the AE-DNN as a loss function for training. The latent (encoded) space of the AE-DNN consists of  $F$  feature measurements denoted by  $\mathbf{z}_{fi,n}^{(j)}$  collected by the vector  $\mathbf{z}_{fn}^{(j)} = [z_{f1,n}^{(j)} \dots z_{fF,n}^{(j)}]^T$ , where  $i$  is the feature index. Since we choose  $F \ll N_s$ , the AE-DNN can be said to compress the information contained in the received signal vector into  $\mathbf{z}_{fn}^{(j)}$ . The encoder-decoder architecture of the AE-DNNs enables unsupervised training using unlabeled samples of baseband signals collected in the set  $\{\mathbf{r}_{n'}^{(j)}\}_{n'=1}^{N'}$ , where  $N'$  is the number of training samples. The stacked vector  $\mathbf{z}_{fn} = [z_{fn}^{(1)T} \dots z_{fn}^{(J)T}]^T$

<sup>2</sup>Note that a low value for  $\gamma$  results in an increased number of false alarms, but allows the detection of low amplitude MPCs. See [60] for determining  $\gamma$  from the desired false alarm probability.

<sup>3</sup>As suggested in [43], we used the magnitudes of the complex baseband signal. However, our work could be extended to complex neural networks along the lines of [62], [63].

is used by the proposed algorithm as an additional noisy measurement.

## IV. FACTOR GRAPH-BASED ALGORITHM

### A. Random Variables and Assumptions

The current state of the agent  $\mathbf{x}_n$  is the primary random variable to be inferred by the proposed factor graph-based algorithm. Additionally, we define the auxiliary state variables  $u_n^{(j)}$ ,  $q_n^{(j)}$ , and  $a_n^{(j)}$ , which denote the normalized amplitude, LOS probability and association variable, respectively, and are modeled separately for all anchors. The presented measurement model consists of a physics-based measurement model, which uses the signal component measurements  $\mathbf{z}_n^{(j)}$  obtained by the CEDA, and a data-driven measurement model, which uses the autoencoder (AE)-based feature measurements  $\mathbf{z}_{fn}^{(j)}$ . Our model is based on the assumptions that

- (I) CEDA-based signal component measurements are uninformative with respect to NLOS components (MPCs)<sup>4</sup>.
- (II) AE-based feature measurements are uninformative with respect to the LOS component<sup>5</sup>.
- (III) CEDA-based measurements and feature-based measurements are conditionally independent for different values of  $m$  [19], [47] and  $i$  [43], [64] given the state variables.

### B. Physics-based Measurement Model

The LOS likelihood function (LHF) of an individual distance measurement  $z_{d_{m,n}^{(j)}}$  is given by

$$f_L(z_{d_{m,n}^{(j)}} | \mathbf{p}_n, u_n^{(j)}) \triangleq f_N(z_{d_{m,n}^{(j)}}; d_{\text{LOS}}^{(j)}(\mathbf{p}_n), \sigma_d(u_n^{(j)})) \quad (2)$$

where  $f_N(\cdot)$  denotes a Gaussian probability density function (PDF) of the random variable (RV)  $z_{d_{m,n}^{(j)}}$  with mean  $d_{\text{LOS}}^{(j)}(\mathbf{p}_n)$  and variance  $\sigma_d^2(u_n^{(j)})$ . The mean is physically related to the agent position via  $d_{\text{LOS}}^{(j)}(\mathbf{p}_n) = \|\mathbf{p}_n - \mathbf{p}_A^{(j)}\|$ . The variance is determined by the Fisher information given by  $\sigma_d^2(u_n^{(j)}) = c^2 / (8\pi^2 \beta_{\text{bw}}^2 u_n^{(j)2})$  [12], where  $\beta_{\text{bw}}$  is the root mean squared bandwidth [1], [65] and  $u_n^{(j)}$  is the normalized amplitude [23], [49]. The LOS LHF of the normalized amplitude measurement  $z_{u_{m,n}^{(j)}}$  is modeled as [45], [49]

$$f_L(z_{u_{m,n}^{(j)}} | u_n^{(j)}) \triangleq f_{\text{TRice}}(z_{u_{m,n}^{(j)}}; \sigma_u(u_n^{(j)}), u_n^{(j)}, \gamma) \quad (3)$$

with  $f_{\text{TRice}}(\cdot)$  being a truncated Rician PDF [23] with non-centrality parameter  $u_n^{(j)}$  and threshold value corresponding to  $\gamma$  (see Sec. III-A). The scale parameter is again determined by the Fisher information and given as  $\sigma_u^2(u_n^{(j)}) = 1/2 + u_n^{(j)2} / (4N_s)$ . See [49] for a detailed derivation. Since we assume CEDA-based measurements to be uninformative with respect to NLOS propagation (Assumption I), the NLOS

<sup>4</sup>Assumption I is commonly used in PDA [50] representing the least informative model for clutter measurements. Although it does not consider the precise statistics of measurements originating from MPCs, it does not affect the estimate as it does not impose curvature on the likelihood model.

<sup>5</sup>Assumption II is not true in LOS situations, which leads to an overconfident estimate (reduced position uncertainty) of the agent posterior. However, this is counteracted by the LOS probability model that “deactivates” the feature-based likelihood in LOS condition by causing the existence probability  $p_E(u_n^{(j)}, q_n^{(j)})$  (see Sec. IV-D) to approach 1.

LHF of an individual distance measurement  $z_{d,m,n}^{(j)}$  is given as [46], [50]  $f_{\text{NL}}(z_{d,m,n}^{(j)}) \triangleq f_{\text{U}}(z_{d,m,n}^{(j)}; 0, d_{\text{max}})$  where  $f_{\text{U}}(\cdot)$  denotes a uniform PDF of the RV  $z_{d,m,n}^{(j)}$  with the limits 0 and  $d_{\text{max}}$  corresponding to the distance measurement range of the CEDA. In correspondence to (3), the NLOS LHF of an individual normalized amplitude measurement  $z_{u,m,n}^{(j)}$  is given as [45], [49]  $f_{\text{NL}}(z_{u,m,n}^{(j)}) \triangleq f_{\text{TRayl}}(z_{u,m,n}^{(j)}; \sqrt{1/2}, \gamma)$  where  $f_{\text{TRayl}}(\cdot)$  is a truncated Rayleigh PDF with scale parameter of  $\sqrt{1/2}$  and threshold value corresponding to  $\gamma$ .

### C. Data-driven Measurement Model

The NLOS LHF of individual feature measurements  $z_{f,i,n}^{(j)}$  is modeled as

$$f_{\text{NL}}(z_{f,i,n}^{(j)} | \mathbf{p}_n) \triangleq f_{\text{N}}(z_{f,i,n}^{(j)}; \mu_{\text{GP}i}^{(j)}(\mathbf{p}_n), \sigma_{\text{GP}i}^{(j)}(\mathbf{p}_n)) \quad (4)$$

with  $\mu_{\text{GP}i}^{(j)}(\mathbf{p}_n)$  and  $\sigma_{\text{GP}i}^{(j)}(\mathbf{p}_n)$  being the predicted mean and predicted variance, respectively, of a Gaussian process regression (GPR) model<sup>6</sup> [55]. We train the GPR model using *labeled* data consisting of duples of feature measurements and according position labels collected in the set  $\{(z_{f,n''}^{(j)}, \mathbf{p}_{n''}^{(j)})\}_{n''=1}^{N''}$ , where  $N''$  is the number of training samples. Since we assume the AE-based feature measurements  $z_{f,i,n}^{(j)}$  to be non-informative with respect to LOS propagation (Assumption II), the LOS LHF of individual  $z_{f,i,n}^{(j)}$  is given by  $f_{\text{L}}(z_{f,i,n}^{(j)}) \triangleq f_{\text{U}}(z_{f,i,n}^{(j)}; l_{\text{mini}}^{(j)}, l_{\text{maxi}}^{(j)})$ , where  $l_{\text{mini}}^{(j)}$  and  $l_{\text{maxi}}^{(j)}$  are the lower and upper limits of the feature measurement range, respectively<sup>7</sup>.

### D. Probabilistic Data Association (PDA) Model

At each time  $n$  and for each anchor  $j$ , the CEDA measurements, i.e., the components of  $\mathbf{z}_n^{(j)}$  are subject to data association uncertainty. Thus, it is not known which measurement  $z_{m,n}^{(j)}$  originated from the LOS, or which one is due to a ‘‘NLOS measurement’’, i.e., a measurement originating from an MPC or a false alarm (FA). Based on the concept of probabilistic data association (PDA) [50], we define the association variable  $a_n^{(j)}$  as

$$a_n^{(j)} = \begin{cases} m \in \mathcal{M}_n^{(j)}, & z_{m,n}^{(j)} \text{ is the LOS measurement in } \mathbf{z}_n^{(j)} \\ 0, & \text{there is no LOS measurement in } \mathbf{z}_n^{(j)} \end{cases} \quad (5)$$

Using no prior knowledge about the mean rate of NLOS measurements (so called ‘‘non-parametric model’’ [50]), the joint probability mass function (PMF) of  $a_n^{(j)}$  and  $M_n^{(j)}$  can be shown to be proportional to the function [50, Sec. 3.4.3]

$$h(a_n^{(j)}, M_n^{(j)}; u_n^{(j)}, q_n^{(j)}) = \begin{cases} \frac{p_{\text{E}}(u_n^{(j)}, q_n^{(j)})}{M_n^{(j)}}, & a_n^{(j)} \in \mathcal{M}_n^{(j)} \\ 1 - p_{\text{E}}(u_n^{(j)}, q_n^{(j)}), & a_n^{(j)} = 0 \end{cases} \quad (6)$$

<sup>6</sup>This choice leads to a computational complexity of the proposed method given as  $\mathcal{O}(N''^2 JIF)$  [55] per time  $n$ , since the GPR-based likelihood function in (4) must be evaluated for each feature, particle, and anchor, which leads to high runtimes for large sets of training data.

<sup>7</sup>For implementation, we normalize the latent variables using the ‘‘pre-training’’ dataset (see Sec. V-A) to obtain the feature-based measurements  $z_{f,i,n}^{(j)}$ , thus,  $l_{\text{mini}}^{(j)} = 0$  and  $l_{\text{maxi}}^{(j)} = 1$  for all  $i$  and  $j$ .

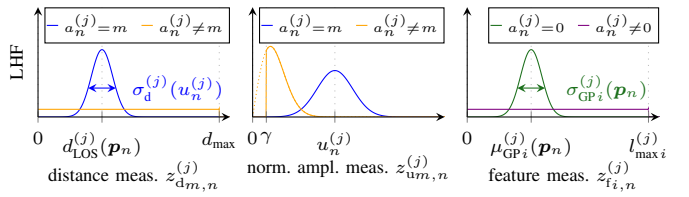


Fig. 2. Graphical representation of the stochastic models constituting the overall LHF for a single measurement.

where the LOS *existence* probability  $p_{\text{E}}(u_n^{(j)}, q_n^{(j)})$  denotes the probability that there is a LOS measurement for the current set of measurements. It is given as  $p_{\text{E}}(u_n^{(j)}, q_n^{(j)}) \triangleq p_{\text{D}}(u_n^{(j)}) q_n^{(j)}$  with  $q_n^{(j)}$  being the probability of the event that the LOS is *not* obstructed, which we refer to as *LOS probability*, and  $p_{\text{D}}(u_n^{(j)})$  being the detection probability, i.e., the probability that at time  $n$  and for anchor  $j$  the agent generates a radio signal component whose amplitude is high enough so that it leads to an LOS measurement. The LOS probability  $q_n^{(j)}$  is modeled as a discrete RV taking its values from the finite set  $\mathcal{Q} = \{\lambda_1, \dots, \lambda_Q\}$ , where  $\lambda_i \in (0, 1]$ . See [23, Sec. IV-D] for details. We also define the joint vector  $\mathbf{a}_n = [a_n^{(1)} \dots a_n^{(J)}]^T$ .

Incorporating  $a_n^{(j)}$  into the model, we define the overall LHF for individual distance measurements, given as

$$f(z_{d,m,n}^{(j)} | \mathbf{p}_n, u_n^{(j)}, a_n^{(j)}) = \begin{cases} f_{\text{L}}(z_{d,m,n}^{(j)} | \mathbf{p}_n, u_n^{(j)}), & a_n^{(j)} = m \\ f_{\text{NL}}(z_{d,m,n}^{(j)}), & a_n^{(j)} \neq m \end{cases} \quad (7)$$

and the overall LHF for individual normalized amplitude measurements, given as

$$f(z_{u,m,n}^{(j)} | u_n^{(j)}, a_n^{(j)}) = \begin{cases} f_{\text{L}}(z_{u,m,n}^{(j)} | u_n^{(j)}), & a_n^{(j)} = m \\ f_{\text{NL}}(z_{u,m,n}^{(j)}), & a_n^{(j)} \neq m \end{cases} \quad (8)$$

We seek to utilize the information contained in the data-driven model (i.e., NLOS information) only in situations where the LOS is not available. Therefore, we define the overall LHF for individual feature measurements as

$$f(z_{f,i,n}^{(j)} | \mathbf{p}_n, a_n^{(j)}) = \begin{cases} f_{\text{NL}}(z_{f,i,n}^{(j)} | \mathbf{p}_n), & a_n^{(j)} = 0 \\ f_{\text{L}}(z_{f,i,n}^{(j)}), & a_n^{(j)} \neq 0 \end{cases} \quad (9)$$

The shapes of (7), (8), and (9) are depicted in Fig. 2. By assuming conditional independence of CEDA-based measurements and feature-based measurements (Assumption I and II) and conditional independence of measurements for different values of  $m$  and  $i$  (Assumption III), the joint LHF for all measurements per anchor  $j$  and time  $n$  is given as

$$\begin{aligned} f(\mathbf{z}_n^{(j)}, \mathbf{z}_{f,n}^{(j)} | \mathbf{p}_n, u_n^{(j)}, a_n^{(j)}) &= \prod_{m=1}^{M_n^{(j)}} f(z_{d,m,n}^{(j)} | \mathbf{p}_n, u_n^{(j)}, a_n^{(j)}) f(z_{u,m,n}^{(j)} | u_n^{(j)}, a_n^{(j)}) \\ &\quad \times \left( \prod_{i=1}^F f(z_{f,i,n}^{(j)} | \mathbf{p}_n, a_n^{(j)}) \right). \end{aligned} \quad (10)$$

### E. State Transition Model

We model the evolution over time  $n$  of  $\mathbf{x}_n$  and  $u_n^{(j)}$  and  $q_n^{(j)}$  as first-order Markov processes which are distributed independently, i.e.,  $f(\mathbf{x}_n, \mathbf{u}_n, \mathbf{q}_n | \mathbf{x}_{n-1}, \mathbf{u}_{n-1}, \mathbf{q}_{n-1}) = f(\mathbf{x}_n | \mathbf{x}_{n-1})$

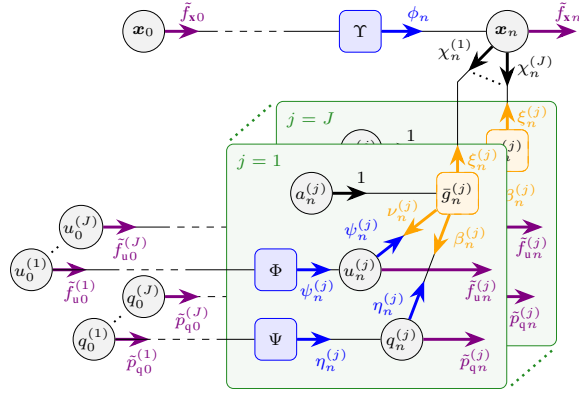


Fig. 3. Factor graph representing the factorization of the joint posterior PDF in (11) and the respective messages according to the SPA. The following short notations are used for the marginal posterior messages:  $\check{f}_{x_n} \triangleq \check{f}_x(\mathbf{x}_n)$ ,  $\check{f}_{y_n}^{(j)} \triangleq \check{f}_y(u_n^{(j)})$ ,  $\check{p}_{q_n}^{(j)} \triangleq \check{p}_q(q_n^{(j)})$ . See [23, Sec. VI] for details regarding the messages  $\eta_n$ ,  $\phi_n$ ,  $\psi_n^{(j)}$ ,  $\xi_n^{(j)}$ ,  $\chi_n^{(j)}$ ,  $\nu_n^{(j)}$ ,  $\beta_n^{(j)}$ , and  $\gamma_n^{(j)}$ .

$\prod_{j=1}^J f(u_n^{(j)}|u_{n-1}^{(j)}) p(q_n^{(j)}|q_{n-1}^{(j)})$  with the joint vectors  $\mathbf{u}_n = [u_n^{(1)} \dots u_n^{(J)}]^\top$ , and  $\mathbf{q}_n = [q_n^{(1)} \dots q_n^{(J)}]^\top$ .

### F. Joint Posterior and Factor Graph

Let  $\mathbf{z}_{1:n} = [\mathbf{z}_1^\top \dots \mathbf{z}_n^\top]^\top$ ,  $\mathbf{z}_{f1:n} = [\mathbf{z}_{f1}^\top \dots \mathbf{z}_{fn}^\top]^\top$ ,  $\mathbf{x}_{1:n} = [\mathbf{x}_1^\top \dots \mathbf{x}_n^\top]^\top$ ,  $\mathbf{a}_{1:n} = [\mathbf{a}_1^\top \dots \mathbf{a}_n^\top]^\top$ ,  $\mathbf{u}_{1:n} = [\mathbf{u}_1^\top \dots \mathbf{u}_n^\top]^\top$ ,  $\mathbf{q}_{1:n} = [\mathbf{q}_1^\top \dots \mathbf{q}_n^\top]^\top$ ,  $\mathbf{M}_{1:n} = [\mathbf{M}_1^\top \dots \mathbf{M}_n^\top]^\top$ . By applying Bayes' rule, the joint posterior PDF of all state variables up to time  $n$  and all  $J$  anchors is given (up to irrelevant constant terms) as

$$f(\mathbf{x}_{1:n}, \mathbf{a}_{1:n}, \mathbf{u}_{1:n}, \mathbf{q}_{1:n}, \mathbf{M}_{1:n} | \mathbf{z}_{1:n}, \mathbf{z}_{f1:n}) \propto f(\mathbf{x}_0) \prod_{j=1}^J p(q_0^{(j)}) f(u_0^{(j)}) \prod_{n'=1}^n \Upsilon(\mathbf{x}_{n'} | \mathbf{x}_{n'-1}) \Phi(u_{n'}^{(j)} | u_{n'-1}^{(j)}) \times \Psi(q_{n'}^{(j)} | q_{n'-1}^{(j)}) \bar{g}(\mathbf{z}_{n'}^{(j)}, \mathbf{z}_{fn'}^{(j)}; \mathbf{p}_{n'}, u_{n'}^{(j)}, a_{n'}^{(j)}, q_{n'}^{(j)}), \quad (11)$$

where we introduced the state-transition functions  $\Upsilon(\mathbf{x}_n | \mathbf{x}_{n-1}) \triangleq f(\mathbf{x}_n | \mathbf{x}_{n-1})$ ,  $\Phi(u_n^{(j)} | u_{n-1}^{(j)}) \triangleq f(u_n^{(j)} | u_{n-1}^{(j)})$ , and  $\Psi(q_n^{(j)} | q_{n-1}^{(j)}) \triangleq p(q_n^{(j)} | q_{n-1}^{(j)})$ . We also introduced the pseudo likelihood function  $\bar{g}(\mathbf{z}_n^{(j)}, \mathbf{z}_{fn}^{(j)}; \mathbf{p}_n, u_n^{(j)}, a_n^{(j)}, q_n^{(j)}) \triangleq h(a_n^{(j)}; u_n^{(j)}, q_n^{(j)}) g(\mathbf{z}_n^{(j)}, \mathbf{z}_{fn}^{(j)}; \mathbf{p}_n, u_n^{(j)}, a_n^{(j)})$ , where we define

$$g(\mathbf{z}_n^{(j)}, \mathbf{z}_{fn}^{(j)}; \mathbf{p}_n, u_n^{(j)}, a_n^{(j)}) \propto f(\mathbf{z}_n^{(j)}, \mathbf{z}_{fn}^{(j)} | \mathbf{p}_n, u_n^{(j)}, a_n^{(j)}) = \begin{cases} \prod_{i=1}^F f_{\text{NL}}(z_{fi,n}^{(j)} | \mathbf{p}_n) / f_{\text{L}}(z_{fi,n}^{(j)}), & a_n^{(j)} = 0 \\ \Lambda(\mathbf{z}_{a_n^{(j)},n}^{(j)} | \mathbf{p}_n, u_n^{(j)}), & a_n^{(j)} \in \mathcal{M}_n^{(j)} \end{cases} \quad (12)$$

by neglecting the constant terms in (10), where

$$\Lambda(\mathbf{z}_{m,n}^{(j)} | \mathbf{p}_n, u_n^{(j)}) = \frac{f_{\text{L}}(z_{dm,n}^{(j)} | \mathbf{p}_n, u_n^{(j)}) f_{\text{L}}(z_{um,n}^{(j)} | u_n^{(j)})}{f_{\text{NL}}(z_{dm,n}^{(j)}) f_{\text{NL}}(z_{um,n}^{(j)})} \quad (13)$$

is the likelihood ratio of signal component measurements<sup>8</sup>. Note that  $\mathbf{M}_{1:n}$  is fixed and thus constant, as it is defined implicitly by the measurements  $\mathbf{z}_{1:n}$ , thus,  $h(a_n^{(j)}; u_n^{(j)}, q_n^{(j)}) \equiv h(a_n^{(j)}, \mathbf{M}_n^{(j)}; u_n^{(j)}, q_n^{(j)})$ . The joint posterior PDF in (11) is represented by the factor graph shown in Fig. 3.

<sup>8</sup>For  $a_n^{(j)} = 0$ , (12) is determined by the likelihood ratio of the feature measurements and, thus, information is gained from the data-driven model. When  $a_n^{(j)} = m \in \mathcal{M}_n^{(j)}$  (not zero), (12) is determined by the likelihood ratio of signal component measurements and, thus, information is gained from the physics-based model w.r.t. the  $m$ -th signal component measurement.

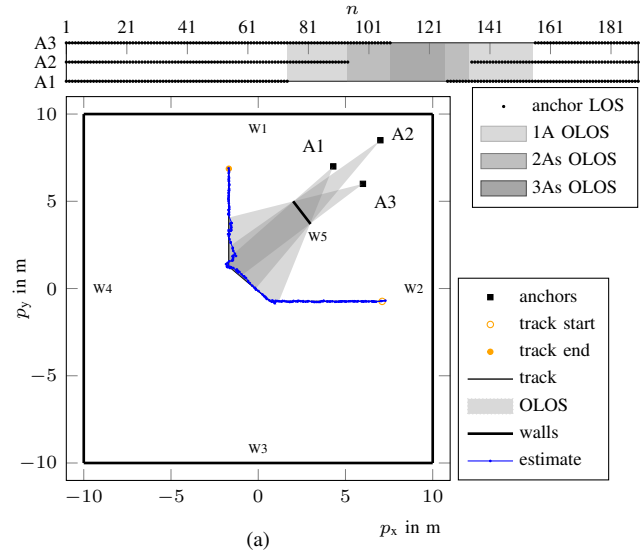


Fig. 4. Graphical representation of the investigated synthetic experiment: Fig. (a) shows the simulated trajectory, anchor positions, walls, and OLOS intervals. Figs. (b) and (c) show the positions of all simulated training datasets.

### G. Algorithm

The problem considered is the sequential estimation of the agent state  $\hat{\mathbf{x}}_n^{\text{MMSE}}$  through the MMSE estimate given by (1). Furthermore, we also calculate MMSE estimates of normalized amplitude  $\hat{u}_n^{(j)\text{MMSE}} \triangleq \int u_n^{(j)} f(u_n^{(j)} | \mathbf{z}_{1:n}, \mathbf{z}_{f1:n}) du_n^{(j)}$  and LOS probability  $\hat{q}_n^{(j)\text{MMSE}} \triangleq \sum_{\omega_i \in \mathcal{Q}} \omega_i p(q_n^{(j)} = \omega_i | \mathbf{z}_{1:n}, \mathbf{z}_{f1:n})$ .

In order to obtain these quantities, the respective marginal posterior PDFs need to be calculated from the joint posterior PDF in (11). In general this is computationally infeasible [47]. Therefore, we use message passing by means of the SPA rules [53] on the factor graph in Fig. 3 that represents a factorization of the joint posterior PDF. Since the integrals involved in the calculations of the SPA messages cannot be obtained analytically, we use a computationally efficient, sequential particle-based implementation that provides approximate results. See [23, Sec. VI] for details concerning SPA, particle-based implementation and the determination of the initial distributions, i.e.,  $f(\mathbf{x}_0)$ ,  $f(u_0^{(j)})$ ,  $p(q_0^{(j)})$ <sup>9</sup>. Note that  $\check{f}_x(\mathbf{x}_n) \propto f(\mathbf{x}_n | \mathbf{z}_{1:n}, \mathbf{z}_{f1:n})$ ,  $\check{f}_y(u_n^{(j)}) \propto f(u_n^{(j)} | \mathbf{z}_{1:n}, \mathbf{z}_{f1:n})$ ,  $\check{p}_q(q_n^{(j)}) \propto p(q_n^{(j)} | \mathbf{z}_{1:n}, \mathbf{z}_{f1:n})$  in Fig. 3 denote the messages

<sup>9</sup>The factorization structure given in [23, Sec. VI] is identical to the problem at hand, when replacing  $\bar{\mathbf{x}}_n$  with  $\mathbf{x}_n$  and  $\bar{\mathbf{y}}_n^{(j)}$  with  $u_n^{(j)}$ . We introduce the additional approximation that the LOS existence probability  $p_E(u_n^{(j)}, q_n^{(j)})$  is only affected by the physics-based model, i.e., when evaluating the messages  $\nu(u_n^{(j)})$ , and  $\beta(q_n^{(j)})$ , we set  $f(z_{fi,n}^{(j)} | \mathbf{p}_n, a_n^{(j)}) \triangleq 1$  for all  $i$ .

corresponding to the marginal posterior distributions.

## V. COMPUTATIONAL RESULTS

### A. Simulation Setup and Scenario

We evaluate the proposed algorithm using synthetic radio measurements, generated according to the scenario presented in Fig. 4a, where the agent moves along a trajectory with two distinct direction changes. It is observed at 190 discrete time steps at a constant observation rate of  $\Delta T = 100$  ms. The ground truth VA positions and corresponding MPC distances are calculated based on the floor plan of Fig. 4a (W1 to W4) using the image source model [21], [66]. The normalized amplitudes of the LOS component as well as the MPCs are assumed to follow free-space path loss according to their individual propagation paths, and are set to 38 dB at a distance of 1 m. The normalized amplitudes of MPCs are additionally attenuated by 3 dB per reflection. The anchors are obstructed by an obstacle (W5), which leads to partial and full OLOS situations in the center of the track. We choose the transmitted signal to be of root-raised-cosine shape with a roll-off factor of 0.6 and a 3-dB bandwidth of 500 MHz. The received baseband signal is critically sampled, i.e.,  $T_s = 1.25$  ns, with a total number of  $N_s = 81$  samples, amounting to a maximum distance  $d_{\max} = 30$  m. We use the CEDA from the supplementary material of [23] with detection threshold of  $\gamma = 2$  (corresponding to 6 dB). The AE-DNN is set up as suggested in [43]: We use feed-forward networks with three convolutional layers for both, encoder and decoder. The encoder is set up as  $27 \times 17$ -ELU,  $27 \times 13$ -ReLU,  $16 \times 5$ -ELU, which denotes the number of convolutional kernels times filter size and the respective activations, and applies max pooling of size 2 after all activation functions. It uses the magnitudes of the baseband signal vector  $|\mathbf{r}_n^{(j)}|$  as an input and has a latent space of 4 variables. The decoder network mirrors the encoder network. For implementation we used Python along with TensorFlow/Keras and optimized using Adam with learning rate of  $2 \cdot 10^{-3}$ , using the MSE of measured and predicted values of  $\mathbf{r}_n^{(j)}$  as loss function. To implement the feature measurement model of (4) we utilized MATLAB's GPR toolbox, where we employed the "Matern52" kernel function [43]. The state transition PDF  $f(\mathbf{x}_n | \mathbf{x}_{n-1})$  of the agent state  $\mathbf{x}_n$  is described by a linear, constant-velocity and stochastic-acceleration model [67, p. 273], given as  $\mathbf{x}_n = \mathbf{A} \mathbf{x}_{n-1} + \mathbf{B} \mathbf{w}_n$  with the acceleration process  $\mathbf{w}_n$  being i.i.d. across  $n$ , zero mean, and Gaussian with covariance matrix  $\sigma_a^2 \mathbf{I}_2$ , the acceleration standard deviation  $\sigma_a$ , and  $\mathbf{A} \in \mathbb{R}^{4 \times 4}$  and  $\mathbf{B} \in \mathbb{R}^{4 \times 2}$  being defined according to [67, p. 273]. The state transition of the normalized amplitude  $u_n$ , i.e., the state transition PDF  $f(u_n | u_{n-1})$ , is chosen as  $u_n^{(j)} = u_{n-1}^{(j)} + \epsilon_{u_n}^{(j)}$ , where the noise  $\epsilon_{u_n}^{(j)}$  is i.i.d. across  $n$ , zero mean, Gaussian, with variance  $\sigma_u^2$ . The state transition variances are set as  $\sigma_a = 2$  m/s<sup>2</sup> and  $\sigma_u = 0.05 \hat{u}_{n-1}^{(j)\text{MMSE}}$ . The set of possible LOS probabilities  $\mathcal{Q}$  and the elements of the state transition PMF  $p(q_n^{(j)} | q_{n-1}^{(j)})$  are set in accordance to [23, Sec. VII-A]. The number of particles to represent the "stacked state"

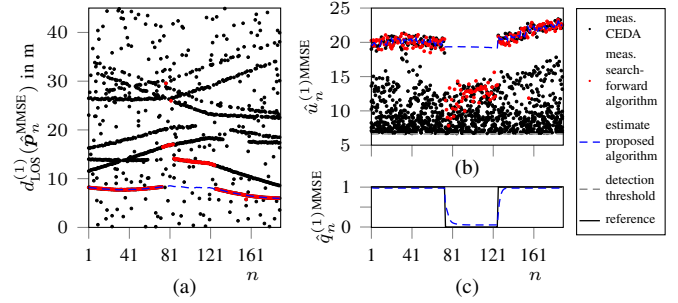


Fig. 5. A single measurement realization and the respective MMSE estimates of the proposed algorithm in (a) distance domain  $d_{\text{LOS}}^{(1)\text{MMSE}}$ , (b) amplitude domain  $\hat{u}_n^{(1)\text{MMSE}}$ , and (c) LOS probability domain  $\hat{q}_n^{(1)\text{MMSE}}$ .

[19], [23], [47, Sec. VI] consisting of all random variables dependent over time  $n$  was set to  $I = 5000$ .

### B. Reference Methods

We compare the performance of the proposed method to a particle-based variant of the multi-sensor amplitude-information PDA (AIPDA) [51], the NLOS cluster based algorithm as presented in [23], and the machine learning based methods from [43] and [15]. Since the methods from [43] and [15] do not perform data association, we estimate the LOS component distance using a search-forward approach [8]. On the interpolated Bartlett spectrum [68], we search for the first maximum that exceeds a threshold, which we chose as six times the noise variance of the received baseband signal. The search-forward approach enables correctly identifying the LOS component (i.e., the first visible signal component), even when there are MPCs with amplitudes higher than that of the LOS component. For the method from [43] we set up the AE-DNN and the GPR with identical configurations as the proposed algorithm (corresponding to the suggestions in [43]). Initial distribution as well as state transition model of the agent state were also set in accordance with the proposed algorithm. To ensure fair comparison, we used Fisher information based variances for the delay likelihood model instead of heuristically set values. Note that this method performs "anomaly detection", i.e., a data-driven identification of OLOS situations, using a beta variational AE-DNN [35] that is implemented using the configuration suggested in [36], [43]<sup>10</sup>. For the method from [15], we provide results using the setup referred to as "GP", which learns a bias correction term using GPR based on the six parametric features suggested by the authors.<sup>11</sup> After error correction of the distance measurements according to

<sup>10</sup>The authors suggest to use feed-forward networks with three dense layers for both, encoder and decoder. The encoder uses the stacked real and imaginary parts of the baseband signal vector as an input. It consists of 100, 80, and 60 neurons, respectively, all with ReLU activation functions, and it has two latent variables. The decoder mirrors the encoder. The regularization hyper parameter is set to  $\beta = 10^{-3}$  and the MSE is used as a data reconstruction loss. As suggested, we used the "time index signal strength indicator" for predicting the anomaly score and compared to the optimum detection threshold being set to the intersection point of the histograms of the agent trajectory data (which is not available in reality).

<sup>11</sup>Note that the approach based on support vector machines (termed "SVM" in [15]) did not yield stable results for the investigated experiment. Using logarithmic features ("log-GP") also did not improve the results, while this variant is prohibitive when negative bias values occur.

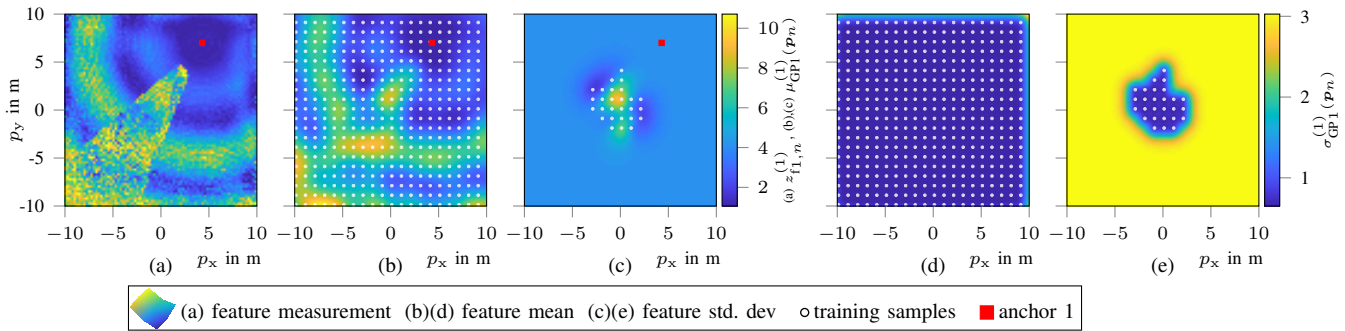


Fig. 6. Exemplary illustration of the latent space representation learned by the AE-DNN in Fig. (a) along with the mapping learned by GPR for feature  $i = 1$  of anchor  $j = 1$ , where Figs. (b) and (c) represent the GPR mean and Figs. (d) and (e) represent the GPR standard deviation for the two datasets shown in Fig. 4b that are used for training of the proposed algorithm. The “full” dataset is used for Figs. (b) and (d) and the “sparse” dataset for Figs. (c) and (e).

[15], for fair comparison, we infer the agent position using a particle filter with identical configuration (initial distributions, state transition model) as the proposed method instead of using the suggested maximum likelihood positioning. Also, in accordance with the proposed method, the likelihood variances are determined from the Fisher information.

### C. Training procedure

Training of the proposed algorithm involves a two step procedure. First, the AE-DNN learns a low dimensional latent representation of the received signal (“pre-training”). We used  $N' = 6400$  unlabeled samples that cover the entire floorplan constituting a two-dimensional grid from  $-10$  m to  $10$  m in  $p_x$  and  $p_y$  directions with  $0.25$  m spacing. Second, GPR is used to learn the mapping in (4). We provide results for two sets of training data as depicted in Fig. 4b: A dataset covering the entire floorplan with  $1$  m grid spacing (“full”) and a small dataset covering only the OLOS regions of the respective anchors (“sparse”).

While the multi-sensor AIPDA and the algorithm from [23] require no training, the method from [43] was trained using the same training data as the proposed algorithm. However, this method additionally requires training of the variational AE-DNN used for “anomaly detection” with LOS only data (i.e., no OLOS situations). We used  $6400$  samples generated at the same positions as for “pre-training” while deactivating the obstructing wall (W5). Training of the method from [15] requires only one set of training data labeled with their respective positions. Here, we instead provide results using the two datasets depicted in Fig. 4c. The “reduced” dataset consists of those positions of the “full” dataset, where the overall received signal power remains within a moderate range. We found a low received signal power to be detrimental for this method leading to strong fluctuations of the distance error for adjacent positions. Additionally, we used an “overfitted” dataset, which contains only data located around the true agent trajectory.

### D. Numerical Results and Performance Analysis

Fig. 5 shows a single measurement realization and respective MMSE estimates of the proposed method. We show measurements obtained using both, the CEDA and the search-forward approach used for the comparison methods. Fig. 6

gives an exemplary illustration of the latent space representation learned by the AE-DNN as well as the corresponding mapping of mean and standard deviation learned by GPR as a function of the agent position  $\mathbf{p}_n$  for the “full” and the “sparse” dataset (see Sec. V-C). It can be observed that the GPR mean values in Fig. 6b and Fig. 6c align well with the abstract feature space. The GPR standard deviations in Fig. 6d and Fig. 6e remain consistently low in the learned regions and increase significantly in areas where no training data is available. Fig. 7 shows the results of the performed numerical simulation. The results are shown in terms of both, the root mean squared error (RMSE) of the estimated agent position over time  $n$  given as  $e_n^{\text{RMSE}} = \sqrt{\mathbb{E}\{\|\hat{\mathbf{p}}_n^{\text{MMSE}} - \mathbf{p}_n\|^2\}}$  and the cumulative frequency of the magnitude error of the estimated agent position, and are evaluated using a numerical simulation with  $500$  realizations.

As a performance benchmark, we provide the Cramér-Rao lower bound (CRLB) for a single position measurement without tracking (“SP-CRLB”) as well as the P-CRLB, considering the dynamic model of the agent state [23], [57]. The “P-CRLB-LOS” is the P-CRLB assuming the LOS component to all anchors is always available.

The RMSE of the proposed algorithm attains or even outperforms the P-CRLB during full OLOS due to the additional information provided by the geometric imprint of the NLOS components and shows consistent performance for both, “full” and “sparse” training data. While the cluster based approach from [23] also reaches the P-CRLB in LOS condition and manages to maintain the track in every single realization, it shows reduced performance during the OLOS situation. The method from [43] cannot attain the P-CRLB in LOS condition as the GPR-based likelihood interferes with the more precise physical model of the LOS component. It performs moderately during the OLOS situation, losing the track in many realizations, showing increased performance when trained with the “full” dataset compared to training with the “sparse” dataset. The reduced performance of the method from [43] in OLOS situation (w.r.t. the proposed algorithm) can be contributed to (i) the purely Gaussian model of the filter, which offers reduced numerical stability w.r.t. the heavy-tailed likelihood of probabilistic data association methods [50] and (ii) the “anomaly detection” method, which showed a high number

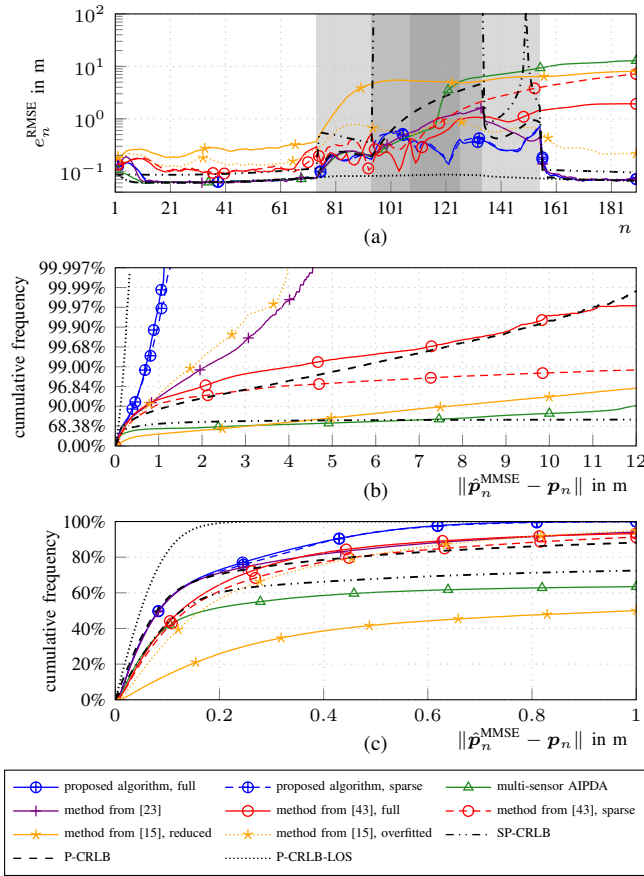


Fig. 7. Performance in terms of the RMSE of the estimated agent position over time  $n$  (a) and as the cumulative frequency of the magnitude error of the estimated agent position in inverse logarithmic scale (b) and linear scale (c). Different shades of gray represent different numbers of anchors in OLOS according to Fig. 4.

of false alarms and missed detections in the investigated experiment. The method from [15], when trained with the “reduced” dataset, shows significantly reduced performance even when the LOS to all anchors is available. It loses the track in many realizations starting at time  $n = 74$  when the LOS to anchor 1 becomes unavailable. When we use the “overfitted” dataset, it manages to perform robustly (i.e., no outliers), confirming its fundamental functionality. However, the RMSE in LOS condition is still significantly reduced. The conventional multi-sensor PDA, which does not facilitate the information contained in MPCs, performs well in LOS condition, but loses track in many realizations during OLOS and follows wrong modes.

## VI. CONCLUSION

We have presented a neural-enhanced sum-product algorithm (SPA) that sequentially estimates the position of a mobile agent using radio signal measurements of multiple anchors by utilizing a hybrid probabilistic model that consists of physics-based and data-driven measurement models embedded in a joint Bayesian framework. We analyzed the performance of the proposed algorithm using numerical simulation in a challenging scenario involving simultaneous obstructed line-of-sight (OLOS) to all anchors. We demonstrated that our algorithm

outperforms state-of-the-art methods for robust positioning and tracking, while consistently attaining the posterior Cramér-Rao lower bound (P-CRLB) (i.e., no lost tracks) even with training data limited to local regions by fusing the information contained in the physics-based and data-driven measurement models.

Possible directions for future research include investigating alternative, uncertainty-aware regression methods for the data-driven measurement model to replace the Gaussian process regression (GPR)-based likelihood function (LHF). These methods should address the challenge of generalization to environments, which are not covered by training data, using concepts such as transfer learning, and should provide an efficient prediction step whose computational complexity does not directly depend on the size of the training data, such as Bayesian neural networks [69].

## ACKNOWLEDGEMENT

The authors thank Dr. Alexander Fuchs and Tobias Gailhofer for valuable discussions during the course of this work.

## REFERENCES

- [1] K. Witrals, P. Meissner *et al.*, “High-accuracy localization for assisted living: 5G systems will turn multipath channels from foe to friend,” *IEEE Signal Process. Mag.*, vol. 33, no. 2, pp. 59–70, Mar. 2016.
- [2] R. Mendrzik, H. Wymeersch, G. Bauch, and Z. Abu-Shaban, “Harnessing NLOS components for position and orientation estimation in 5G Millimeter Wave MIMO,” *IEEE Trans. Wireless Commun.*, vol. 18, no. 1, pp. 93–107, 2019.
- [3] Y. Wang, K. Gu, Y. Wu, W. Dai, and Y. Shen, “NLOS effect mitigation via spatial geometry exploitation in cooperative localization,” *IEEE Trans. Wireless Commun.*, vol. 19, no. 9, pp. 6037–6049, 2020.
- [4] R. Karlsson and F. Gustafsson, “The future of automotive localization algorithms: Available, reliable, and scalable localization: Anywhere and anytime,” *IEEE Signal Process. Mag.*, vol. 34, no. 2, pp. 60–69, 2017.
- [5] J. Ko, T. Gao, R. Rothman, and A. Terzis, “Wireless sensing systems in clinical environments: Improving the efficiency of the patient monitoring process,” *IEEE Eng. Med. Biol. Mag.*, vol. 29, pp. 103–9, 05 2010.
- [6] A. Kalyanaraman, Y. Zeng, S. Rakshit, and V. Jain, “CaraoKey : Car states sensing via the ultra-wideband keyless infrastructure,” in *Proc. IEEE SECON-20*, 2020, pp. 1–9.
- [7] A. Conti, F. Morselli, Z. Liu, S. Bartoletti, S. Mazuelas, W. C. Lindsey, and M. Z. Win, “Location awareness in beyond 5G networks,” *IEEE Commun. Mag.*, vol. 59, no. 11, pp. 22–27, 2021.
- [8] D. Dardari, A. Conti, U. Ferner, A. Giorgetti, and M. Z. Win, “Ranging with ultrawide bandwidth signals in multipath environments,” *Proc. IEEE*, vol. 97, no. 2, pp. 404–426, Feb. 2009.
- [9] L. Taponecco, A. D’Amico, and U. Mengali, “Joint TOA and AOA estimation for UWB localization applications,” *IEEE Trans. Wireless Commun.*, vol. 10, no. 7, pp. 2207–2217, 2011.
- [10] F. Rusek, D. Persson, B. K. Lau, E. G. Larsson, T. L. Marzetta, O. Edfors, and F. Tufvesson, “Scaling up MIMO: Opportunities and challenges with very large arrays,” *IEEE Signal Process. Mag.*, vol. 30, no. 1, pp. 40–60, Jan. 2013.
- [11] A. Richter, “Estimation of Radio Channel Parameters: Models and Algorithms,” Ph.D. dissertation, Ilmenau University of Technology, 2005.
- [12] Y. Shen and M. Z. Win, “Fundamental limits of wideband localization-part I: A general framework,” *IEEE Trans. Inf. Theory*, vol. 56, no. 10, pp. 4956–4980, 2010.
- [13] S. Aditya, A. F. Molisch, and H. M. Behairy, “A survey on the impact of multipath on wideband time-of-arrival based localization,” *Proc. IEEE*, vol. 106, no. 7, pp. 1183–1203, 2018.
- [14] W. M. Gifford, D. Dardari, and M. Z. Win, “The impact of multipath information on time-of-arrival estimation,” *IEEE Trans. Signal Process.*, vol. 70, pp. 31–46, 2022.
- [15] H. Wymeersch, S. Marano, W. M. Gifford, and M. Z. Win, “A machine learning approach to ranging error mitigation for UWB localization,” *IEEE Trans. Wireless Commun.*, vol. 60, no. 6, pp. 1719–1728, 2012.
- [16] C. Gentner, T. Jost, W. Wang, S. Zhang, A. Dammann, and U. C. Fiebig, “Multipath assisted positioning with simultaneous localization and mapping,” *IEEE Trans. Wireless Commun.*, vol. 15, no. 9, pp. 6104–6117, Sep. 2016.

- [17] A. Shahmansoori, G. E. Garcia, G. Destino, G. Seco-Granados, and H. Wymeersch, "Position and orientation estimation through mm Wave MIMO in 5G systems," *IEEE Trans. Wireless Commun.*, vol. 17, no. 3, pp. 1822–1835, Mar. 2018.
- [18] E. Leitinger, F. Meyer, P. Meissner, K. Witrisal, and F. Hlawatsch, "Belief propagation based joint probabilistic data association for multipath-assisted indoor navigation and tracking," in *Proc. ICL-GNSS-16*, Barcelona, Spain, June 2016, pp. 1–6.
- [19] E. Leitinger, F. Meyer, F. Hlawatsch, K. Witrisal, F. Tufvesson, and M. Z. Win, "A belief propagation algorithm for multipath-based SLAM," *IEEE Trans. Wireless Commun.*, vol. 18, no. 12, pp. 5613–5629, 2019.
- [20] H. Kim, K. Granström, L. Gao, G. Battistelli, S. Kim, and H. Wymeersch, "5G mmWave cooperative positioning and mapping using multi-model PHD filter and map fusion," *IEEE Trans. Wireless Commun.*, vol. 19, no. 6, pp. 3782–3795, Mar. 2020.
- [21] T. Pedersen, "Modeling of path arrival rate for in-room radio channels with directive antennas," *IEEE Trans. Antennas Propag.*, vol. 66, no. 9, pp. 4791–4805, 2018.
- [22] S. Jiang, W. Wang, Y. Miao, W. Fan, and A. F. Molisch, "A survey of dense multipath and its impact on wireless systems," vol. 3, pp. 435–460, 2022.
- [23] A. Venus, E. Leitinger, S. Tertinek, and K. Witrisal, "A graph-based algorithm for robust sequential localization exploiting multipath for obstructed-LOS-bias mitigation," *IEEE Trans. Wireless Commun.*, 2023.
- [24] H. Wymeersch, J. Lien, and M. Z. Win, "Cooperative localization in wireless networks," *Proc. IEEE*, vol. 97, no. 2, pp. 427–450, Feb. 2009.
- [25] J. Kulmer, E. Leitinger, S. Grebien, and K. Witrisal, "Anchorless cooperative tracking using multipath channel information," *IEEE Trans. Wireless Commun.*, vol. 17, no. 4, pp. 2262–2275, Apr. 2018.
- [26] M. Chiani, A. Giorgetti, and E. Paolini, "Sensor radar for object tracking," *Proc. IEEE*, vol. 106, no. 6, pp. 1022–1041, 2018.
- [27] S. Marano and W. Gifford, H. Wymeersch, and M. Win, "NLOS identification and mitigation for localization based on UWB experimental data," *IEEE J. Sel. Areas Commun.*, vol. 28, no. 7, pp. 1026–1035, Sept. 2010.
- [28] F. Meyer, Z. Liu, and M. Z. Win, "Network localization and navigation using measurements with uncertain origin," in *Proc. FUSION-18*, July 2018, pp. 1–7.
- [29] Z. Yu, Z. Liu, F. Meyer, A. Conti, and M. Z. Win, "Localization based on channel impulse response estimates," in *Proc. IEEE/ION PLANS-20*, 2020, pp. 1014–1021.
- [30] A. Venus, E. Leitinger, S. Tertinek, and K. Witrisal, "A message passing based adaptive PDA algorithm for robust radio-based localization and tracking," in *2021 Proc. IEEE RadarConf-21*, 2021, pp. 1–6.
- [31] S. Bartoletti, A. Giorgetti, M. Win, and A. Conti, "Blind Selection of Representative Observations for Sensor Radar Networks," *IEEE Trans. Vehicular Technology*, vol. 64, no. 4, pp. 1388–1400, April 2015.
- [32] S. Mazuelas, A. Conti, J. C. Allen, and M. Z. Win, "Soft range information for network localization," *IEEE Trans. Signal Process.*, vol. 66, no. 12, pp. 3155–3168, June 2018.
- [33] A. Conti, S. Mazuelas, S. Bartoletti, W. C. Lindsey, and M. Z. Win, "Soft information for localization-of-things," *Proc. IEEE*, vol. 107, no. 11, pp. 2240–2264, Nov. 2019.
- [34] L. Wielandner, A. Venus, T. Wilding, and E. Leitinger, "Multipath-based SLAM for non-ideal reflective surfaces exploiting multiple-measurement data association," 2023.
- [35] D. P. Kingma and M. Welling, "Auto-encoding variational bayes," in *Proc. ICLR-14*, Banff, AB, Canada, Apr. 2014.
- [36] M. Stahlke, S. Kram, F. Ott, T. Feigl, and C. Mutschler, "Estimating TOA reliability with variational autoencoders," *IEEE Sensors J.*, pp. 1–1, 2021.
- [37] T. Wang, K. Hu, Z. Li, K. Lin, J. Wang, and Y. Shen, "A semi-supervised learning approach for UWB ranging error mitigation," *IEEE Wireless Commun. Lett.*, vol. 10, no. 3, pp. 688–691, 2021.
- [38] Y. Li, S. Mazuelas, and Y. Shen, "A semi-supervised learning approach for ranging error mitigation based on UWB waveform," in *Proc. IEEE MILCOM-21*, 2021, pp. 533–537.
- [39] S. Kadambi, A. Behboodi, J. B. Soriaga, M. Welling, R. Amiri, S. Yerramalli, and T. Yoo, "Neural RF SLAM for unsupervised positioning and mapping with channel state information," in *Proc. IEE ICC-22*, Aug. 2022, pp. 3238–3244.
- [40] Y. Huang, S. Mazuelas, F. Ge, and Y. Shen, "Indoor localization system with NLOS mitigation based on self-training," *IEEE Trans. Mobile Comput.*, pp. 1–1, 2022.
- [41] M. Liang and F. Meyer, "Neural enhanced belief propagation for data association in multiobject tracking," in *Proc. Fusion-22*, Aug. 2022, pp. 1–7.
- [42] —, "Neural enhanced belief propagation for cooperative localization," in *Proc. IEEE SSP-21*, Aug. 2021, pp. 326–330.
- [43] S. Kram, C. Kraus, T. Feigl, M. Stahlke, J. Robert, and C. Mutschler, "Position tracking using likelihood modeling of channel features with Gaussian processes," *ArXiv e-prints*, vol. abs/2203.13110, 2022. [Online]. Available: <http://arxiv.org/abs/2203.13110>
- [44] J. Pinto, G. Hess, W. Ljungbergh, Y. Xia, H. Wymeersch, and L. Svensson, "Deep learning for model-based multi-object tracking," *IEEE Trans. Aerosp. Electron. Syst.*, pp. 1–17, 2023.
- [45] E. Leitinger, S. Grebien, and K. Witrisal, "Multipath-based SLAM exploiting AoA and amplitude information," in *Proc. IEEE ICCW-19*, Shanghai, China, May 2019, pp. 1–7.
- [46] Y. Bar-Shalom, F. Daum, and J. Huang, "The probabilistic data association filter," *IEEE Control Syst. Mag.*, vol. 29, no. 6, pp. 82–100, Dec 2009.
- [47] F. Meyer, T. Kropfreiter, J. L. Williams, R. Lau, F. Hlawatsch, P. Braca, and M. Z. Win, "Message passing algorithms for scalable multitarget tracking," *Proc. IEEE*, vol. 106, no. 2, pp. 221–259, Feb. 2018.
- [48] F. Meyer and J. L. Williams, "Scalable detection and tracking of geometric extended objects," *IEEE Trans. Signal Process.*, vol. 69, pp. 6283–6298, 2021.
- [49] X. Li, E. Leitinger, A. Venus, and F. Tufvesson, "Sequential detection and estimation of multipath channel parameters using belief propagation," *IEEE Trans. Wireless Commun.*, vol. 21, no. 10, pp. 8385–8402, Apr. 2022.
- [50] Y. Bar-Shalom and X.-R. Li, *Multitarget-Multisensor Tracking: Principles and Techniques*. Storrs, CT, USA: Yaakov Bar-Shalom, 1995.
- [51] S. Jeong and J. Tugnait, "Multisensor tracking of a maneuvering target in clutter using IMM-PDA filtering with simultaneous measurement update," *IEEE Trans. Aerosp. Electron. Syst.*, vol. 41, no. 3, pp. 1122–1131, Nov. 2005.
- [52] D. Lerro and Y. Bar-Shalom, "Automated tracking with target amplitude information," in *1990 American Control Conference*, May 1990, pp. 2875–2880.
- [53] F. Kschischang, B. Frey, and H.-A. Loeliger, "Factor graphs and the sum-product algorithm," *IEEE Trans. Inf. Theory*, vol. 47, no. 2, pp. 498–519, Feb. 2001.
- [54] M. A. Kramer, "Nonlinear principal component analysis using autoassociative neural networks," *AICHe Journal*, vol. 37, no. 2, pp. 233–243, 1991.
- [55] C. E. Rasmussen and C. K. I. Williams, *Gaussian processes for machine learning*. MIT Press, 2006.
- [56] G. Soldi, F. Meyer, P. Braca, and F. Hlawatsch, "Self-tuning algorithms for multisensor-multitarget tracking using belief propagation," *IEEE Trans. Signal Process.*, vol. 67, no. 15, pp. 3922–3937, Aug. 2019.
- [57] P. Tichavsky, C. Muravchik, and A. Nehorai, "Posterior Cramer-Rao bounds for discrete-time nonlinear filtering," *IEEE Trans. Signal Process.*, vol. 46, no. 5, pp. 1386–1396, May 1998.
- [58] S. Kay, *Fundamentals of Statistical Signal Processing: Estimation Theory*. Upper Saddle River, NJ, USA: Prentice Hall, 1993.
- [59] M. A. Badiu, T. L. Hansen, and B. H. Fleury, "Variational Bayesian inference of line spectra," *IEEE Trans. Signal Process.*, vol. 65, no. 9, pp. 2247–2261, May 2017.
- [60] E. Leitinger, S. Grebien, B. H. Fleury, and K. Witrisal, "Detection and estimation of a spectral line in MIMO systems," in *Proc. Asilomar-20*, Pacific Grove, CA, USA, Oct. 2020, pp. 1090–1095.
- [61] M. Kramer, "Autoassociative neural networks," *Computers and Chemical Engineering*, vol. 16, no. 4, pp. 313–328, 1992, neural network applications in chemical engineering.
- [62] A. Hirose, *Complex-valued neural networks*. Springer Science & Business Media, 2012, vol. 400.
- [63] C. Trabelsi, O. Bilaniuk, Y. Zhang, D. Serdyuk, S. Subramanian, J. F. Santos, S. Mehri, N. Rostamzadeh, Y. Bengio, and C. J. Pal, "Deep complex networks," in *Internat. Conf. on Learn. Represent. (ICLR)*, 2017.
- [64] Y. Zhao, F. Yin, F. Gunnarsson, M. Amirijoo, and G. Hendeby, "Gaussian process for propagation modeling and proximity reports based indoor positioning," in *Proc. IEEE VTC-16*, 2016, pp. 1–5.
- [65] E. Leitinger, P. Meissner, C. Ruedisser, G. Dumphart, and K. Witrisal, "Evaluation of position-related information in multipath components for indoor positioning," *IEEE J. Sel. Areas Commun.*, vol. 33, no. 11, pp. 2313–2328, Nov. 2015.
- [66] P. Meissner, "Multipath-Assisted Indoor Positioning," Ph.D. dissertation, Graz University of Technology, 2014.
- [67] Y. Bar-Shalom, T. Kirubarajan, and X.-R. Li, *Estimation with Applications to Tracking and Navigation*. New York, NY, USA: John Wiley & Sons, Inc., 2002.
- [68] H. Krim and M. Viberg, "Two decades of array signal processing research: the parametric approach," *IEEE Signal Process. Mag.*, vol. 13, no. 4, pp. 67–94, 1996.
- [69] D. J. MacKay, "A practical Bayesian framework for backpropagation networks," *Neural computation*, vol. 4, no. 3, pp. 448–472, 1992.